



UNIVERSITÀ POLITECNICA DELLE MARCHE  
Repository ISTITUZIONALE

## Comparison between the wintertime and summertime dynamics of the Misa River estuary

This is the peer reviewed version of the following article:

*Original*

Comparison between the wintertime and summertime dynamics of the Misa River estuary / Brocchini, Maurizio; Calantoni, Joseph; Postacchini, Matteo; Sheremet, Alex; Staples, Tracy; Smith, Joseph; Reed, Allen H.; Braithwaite III, Edward F.; Lorenzoni, Carlo; Russo, Aniello; Corvaro, Sara; Mancinelli, Alessandro; Soldini, Luciano. - In: MARINE GEOLOGY. - ISSN 0025-3227. - STAMPA. - 385:(2017), pp. 27-40. [10.1016/j.margeo.2016.12.005]

*Availability:*

This version is available at: 11566/247010 since: 2022-06-06T10:08:25Z

*Publisher:*

*Published*

DOI:10.1016/j.margeo.2016.12.005

*Terms of use:*

The terms and conditions for the reuse of this version of the manuscript are specified in the publishing policy. The use of copyrighted works requires the consent of the rights' holder (author or publisher). Works made available under a Creative Commons license or a Publisher's custom-made license can be used according to the terms and conditions contained therein. See editor's website for further information and terms and conditions.

This item was downloaded from IRIS Università Politecnica delle Marche (<https://iris.univpm.it>). When citing, please refer to the published version.

(Article begins on next page)

# **Comparison between the wintertime and summertime dynamics of the Misa River estuary**

Maurizio Brocchini<sup>a,b</sup>, Joseph Calantoni<sup>c</sup>, Matteo Postacchini<sup>a,\*</sup>, Alex Sheremet<sup>d</sup>, Tracy Staples<sup>d</sup>,  
Joseph Smith<sup>e</sup>, Allen H. Reed<sup>c</sup>, Edward F. Braithwaite III<sup>c</sup>, Carlo Lorenzoni<sup>a</sup>, Aniello Russo<sup>a,b,#</sup>,  
Sara Corvaro<sup>a</sup>, Alessandro Mancinelli<sup>a</sup>, Luciano Soldini<sup>a</sup>

<sup>a</sup> Università Politecnica delle Marche, Ancona, Italy

<sup>b</sup> CoNISMa ULR Ancona, Ancona, Italy

<sup>c</sup> Naval Research Laboratory, Stennis Space Center, MS, USA

<sup>d</sup> University of Florida, Gainesville, FL, USA

<sup>e</sup> Oceanography Department, U. S. Naval Academy, Annapolis, MD, USA

<sup>#</sup> present address: Centre for Maritime Research & Experimentation, La Spezia, Italy

<sup>\*</sup> Corresponding Author: m.postacchini@univpm.it

## ABSTRACT

The Misa River on the Italian Adriatic coast, is typical of the rivers that drain the Apennine Mountain range. The focus of this study, conducted in the late summer of 2013 and mid-winter of 2014, was to contrast the general wintertime-summertime dynamics in the Misa River estuarine system rather than investigate specific dynamical features (e.g. offshore sediment transport, channel seiche, and flocculation mechanisms). Summertime conditions of the Misa River estuary are characterized by low freshwater discharge and net sediment deposition whereas, in the wintertime, the Misa River and estuary is characterized by high episodic freshwater discharge and net erosion and sediment export. Major observed differences between wintertime-summertime dynamics in the Misa River and estuary are a result of seasonal-scale differences in regional precipitation and forcing conditions driven largely by the duration and intensity of prevailing wind patterns that frequently change direction in summertime while keep almost constant directions for much longer periods in wintertime, thus generating major sea storms. Sediment deposition was observed in the final reach of the Misa River and estuary in the summertime. However, in the wintertime, large flood events led to sediment erosion and export in the final reach of the Misa River and estuary that, in conjunction with storm-wave-induced mud transport, led to sediment deposition at the river entrance and in the adjacent nearshore region. The seasonal cyclic pattern of erosion and deposition was confirmed with bathymetric surveys of the final reach of the estuarine region. A critical component for the balance between summertime deposition and wintertime erosion was the presence of an underlying mat of organic deposits that limited the availability of sediments for erosion in winter, when massive debris transport occurs. Further, suspended cohesive sediments flocs were subjected to smaller hydrodynamic stresses in the summertime favoring deposition within the estuary. Conversely,

during wintertime storms, flocs were subjected to larger hydrodynamic stresses favoring breakup into smaller flocs favoring deposition outside the estuary.

KEYWORDS: cohesive sediment transport, estuary, river, morphodynamics, currents, waves

## **1. Introduction**

Large amounts of organic matter and suspended particulate materials are delivered to coastal waters at the deltas of major river systems (Milliman and Syvitski, 1992). The sediment plumes from river systems have acoustic (e.g., see Thorne et al., 2007; Thorne and Hurther, 2014) and optical (e.g., see Manning and Dyer, 2002; Manning, 2004) properties distinct from the ambient receiving waters, which makes the plumes easy to track. Additionally, the suspended sediments in the plumes increase fluid density and viscosity impacting local hydrodynamics. The large suspended load delivered by these rivers can significantly alter the morphology and rheology of the sediment bed (Schindler et al., 2015), which may lead to dampening of incoming waves and reduction of wave breaking as deposited sediments are resuspended during high energy events (e.g., Calliari et al., 2001; Rogers and Holland, 2009).

Fine-grained sediment deposition, accumulation, and transport in riverine-coastal systems can be spatially and temporally heterogeneous due to short-to-medium term changes in: sediment supply; tidal variations on ebb-flood and spring-neap tidal scales; seasonal scale changes in river flow; anthropogenic disturbances; and natural episodic events (Woodruff et al., 2001; Smith et al., 2009). Although there is a general understanding of fine-particle transport and accumulation processes in estuarine systems (Olsen et al., 1993; Smith et al., 2009), measurements and modeling of fine-grained sediment dynamics in coastal regions over significant spatial-temporal scales are extremely difficult because variability in local geologic, hydrodynamic and

physicochemical processes interact to create the following difficulties: 1) fine-particle transport may involve long term suspension of particles as well as numerous short-term episodes of deposition and resuspension (Sanford, 1992; Sanford and Maa, 2001); 2) chemical and biological processes interact at a wide-range of scales to govern the dispersal and fate of sedimentary particles in organic matter-rich zones where ionic strength changes dramatically as freshwater interacts with seawater; and, 3) hydrodynamics are highly variable and episodic events, such as intense storms, are often significantly more important than events that occur on a regular basis during normal flow. Flocculation, in particular, complicates sediment dynamics in river-estuary-coastal systems. Flocculation is the combined process of aggregation and disaggregation of particles, colloids, and dissolved constituents within a water column (Whitehouse et al., 2000; Winterwerp, 2002; Manning, 2004; Mehta, 2014). Flocculation affects particle size distributions in the water column, particle settling rates, and is an important process in the removal of both organic and inorganic materials from the water column to the sediments. Flocculation processes play a key role in determining the strength, density, and cohesion of aggregates after deposition and accumulation in the sediments. Spatial and temporal differences in the flocculation processes occurring with depth along the river-estuarine-coastal gradient alter the acoustic and optical properties of the water column.

Important aspects of flocculation processes deals with mixed fine-grained sediment suspension. Recent studies reveal that natural mud and cohesive sediments (e.g., used as tracers) with similar properties, lead to flocs of completely different characteristics (e.g. settling velocity) with respect to natural muddy material (e.g., Spencer et al., 2010). Further, properties of micro- and macro-flocs are strictly connected to the percentage of suspended materials (sand, silt, clay) within the water column (Whitehouse and Manning, 2007; Manning et al., 2010, 2013), this

being captured by recent empirical and numerical models able at reproducing the dynamics of sand-mud mixtures (Manning et al., 2011; Spearman et al., 2011).

Recent studies demonstrate the importance of cohesion in the bed morphology of estuarine environments. Physical cohesion is fundamental in bedform characterization: the larger is the clay content, the milder is the bed change (e.g., see Schindler et al., 2015). The biological contribution is also important: cohesion often comes from microorganisms which generate biologically cohesive extracellular polymeric substances (EPS). Similar to the physical cohesion, but with more pronounced effects, the biological cohesion increases the erosion threshold and significantly affects the sediment stability, hence controlling the bedform dynamics (e.g., Malarkey et al., 2015; Parsons et al., 2016).

In September, 2013 and January, 2014, we conducted summertime and wintertime field sampling campaigns at the mouth of the Misa River (located in the Marche region, Ancona Province of Italy, MR hereafter) in Senigallia, Italy. The Misa River originates in the Apennine Mountains and discharges into the Western Adriatic Sea. The summertime experiment was used to establish a baseline low-flow/low-energy condition for the lower MR estuary system and river mouth. The January 2014 wintertime campaign on the MR consisted of field studies in the riverine, estuarine, and coastal provinces, where hydrodynamic data, sediment and suspended matter samples, and water column profile data were collected prior to and between the passage of two winter storms. Results presented here focus on the observations from the wintertime campaign with discussion focused on comparisons and contrast between the general wintertime and summertime conditions in the MR-estuarine coastal system. The Misa River may be seen as representative of the majority of the rivers debouching into the Western Adriatic Sea. The presented results will provide the setting for regional-scale comprehension of general sediment

dynamics with some discussion about specific mechanisms and factors that influence sediments dynamics in Apennine rivers like the MR that will be explored in future dedicated works.

The regional setting is described in Section 2, where the MR and its estuary are geologically and hydrologically characterized, together with the sediment transport along the river. Section 3 describes the equipment used during the experiments and the methods of analysis used. The main results (hydrodynamics, morphological changes, sediment transport) of the wintertime campaign are presented in Section 4. In the following discussion (Section **Errore. L'origine riferimento non è stata trovata.**), comparisons were made with the data previously collected during the summertime experiment (Brocchini et al., 2015), showing a fairly different behavior of the final reach and estuary in summer and winter, with low-flow conditions promoting sediment/flocs deposition and the high-flow conditions promoting: i) riverbed erosion, ii) large sediment suspension and development of the river plume, iii) complex morphological patterns at the mouth, due to convergence of sea and river forcing. Some conclusions are presented in Section 6.

## **2. Regional Setting**

Two field experiments were carried out along the final reach of the MR and in the nearshore region in front of the estuary (**Figure 1**). The MR runs for about 48 km from the “Appennino umbro-marchigiano” (central Italy) to the municipality of Senigallia (Marche Region), one of the most important touristic towns of the Italian Middle Adriatic coast. The watershed extension of the MR is 383 km<sup>2</sup>, with discharges of about 400, 450, and 600 m<sup>3</sup> s<sup>-1</sup> for return periods of 100, 200, and 500 years, respectively. Following the classical definition of an estuary, the place where the tide overlaps with the current of a stream, the MR is characteristic of a salt-wedge estuary (Kennish, 1986), where the river forcing prevails on both marine and tidal

influence. Such an estuary type is usually characterized by a fresh water layer over seawater thinning while flowing seaward.

The micro-tidal conditions make it an excellent environment to study the effects of the coupling between river discharge and nearshore hydrodynamics (waves and wave driven currents) on sediment dynamics and the resulting morphodynamics. Additionally, the zone around the MR estuary (**Figure 1a**), within the town of Senigallia (Italy), is heavily engineered having cement walls comparable to a field-scale laboratory flume (**Figure 1b-c**). The beach to the north of the MR estuary is engineered with breakwaters, while the beach to the south is a natural open coast.

## **2.1. Hydrological and geological overview**

The MR is typical of many coastal streams that drain the Apennine Mountains of central Italy into the Adriatic Sea. The Apennine Mountains are comprised of brittle sedimentary rocks, remnants of the Tethys Sea, which are highly extended and heavily fractured (Doglioni et al., 1994). Consequently, the mountain surfaces are easily eroded and supply relatively large quantities of gravel and sediment to the Adriatic Sea (Milliman and Syvetski, 1992). The MR exemplifies the transport process that is common within Apennine Mountain rivers. While relatively small in size, it distributes large quantities of sediment. Sediment mineralogy reflects the characteristics of the sedimentary source materials that dominate the Apennine Mountains such as limestone, shale, and sandstone. An important addition to this diverse mix of minerals is derived from volcanic ash, which was transported from the southeast by winds during the Plinian and other volcanic eruptions (e.g. Rolandi et al., 2008). The deposition of volcanic ash has weathered to form a relatively abundant supply of montmorillonite clays. A similar array of sediment deposits was evident in the alluvial layers that underlie the town of Senigallia where



sediment cores were collected by Favali et al. (1995). The cores displayed layers of muddy sediments that are interspersed with gravel, all of which overlie the bedrock of fractured and faulted mud-, silt- and sandstone.

## **2.2. Sediment transport and deposition**

An important aspect of the sediments of the lower MR estuary is that they display a large concentration of montmorillonite clay minerals indicative of allochthonous materials derived from the Apennine Mountains. These fine-grained clay sediments are retained, often temporarily, or seasonally, within the estuarine area and under the plume due to aggregation of individual clay particles, and perhaps organic matter, into flocs. The larger clay flocs settle out of the water column at a much higher rate than that of the individual, non-aggregated clay particles (e.g. Milligan et al. 2007). Clay sediments are typically deposited rapidly within rivers and near river mouths in fairly shallow depths, <4 m, as clay concentrations and turbulent kinetic energy often promote the development of large flocs that settle at rates of up to  $1 \text{ mm s}^{-1}$  (Fox et al., 2004). These flocs contribute to a thick sequence of muddy sediments that dominate the estuarine portion of the riverbed surface during the low-flow conditions typical of the summertime.

The high stress conditions that promote transport from the Apennines through the coastal rivers and into the littoral zone are enhanced by heavy rains which typically occur in the wintertime (Milliman and Syvitski, 1992) as the frequency and intensity of Bora winds (i.e., cool dry air masses flowing out of northern Ukraine/Siberia into the northern Adriatic through the Dinaric Alps), increase and as the temperature difference between the Scirocco winds and air masses in the northern Adriatic increases. The rains occur due to the interaction of two different climatic systems. One system occurs when the Bora wind interacts with a low pressure cell that is centered over the southern Adriatic and Mediterranean Seas (e.g., see Camuffo, 1984; Horvath

et al., 2008). The second rain producing system occurs when the warm Scirocco wind flows out of Africa, absorbs moisture as it passes over the Mediterranean, and creates rain in the mountains that border the Adriatic Sea (Camuffo, 1984). The average rainfall over the Apennine mountain region during winter is estimated to be 65-84 mm/month (weather station of L'Aquila, one of the main towns of the Apennines) whereas the average rainfall in summer is 35-46 mm/month (<http://cetemps.aquila.infn.it/>).

### **3. Materials and methods**

The first of two experimental campaigns was carried out during the summertime in September 2013 (Brocchini et al., 2015). The summertime experiment was smaller in scope and duration than the primary wintertime experiment executed from 20-31 January 2014. Both experiments were located at the MR estuary and included observations of meteorology, hydrodynamics, and morphodynamics. Additionally, water column profile data and discrete water, suspended matter, and sediment samples were collected from a small boat as weather conditions permitted. Consequently, during the wintertime experiment three days of water and sediment sampling occurred on 26, 27, and 29 January 2014 within the river, estuary and plume, which extended more than 1.3 km offshore during the maximum flow. Sampling was conducted between two winter storms that occurred on 25 and 28 January 2014, respectively. The details of the summertime data collection were previously described (Brocchini et al., 2015).

#### **3.1. Meteorology**

During the wintertime experiment, meteorological data (wind speed and direction, rain, and relative humidity) were logged with a Davis Vantage Pro 2 station installed on the Senigallia harbor lighthouse (location shown in **Figure 1**). Both mean and maximum values collected during 15-minute intervals were recorded by the instrument. Atmospheric pressure and tidal

observations at the Ancona harbor (about 30 km to the south of Senigallia) confirmed the presence of low-pressure dominated storm events during the end of January 2014. The measured storm surge did not always oscillate around the zero level (representing atmospheric pressure of 1013 hPa), as expected from tidal predictions. The three most energetic events occurred on: 1) 21 January 2014 between 01:00-02:00 UTC; 2) 25 January 2014 between 03:00-05:00 UTC; and 3) 28 January 2014 between 07:00-08:00 UTC. The last two of the three events were captured by the *in-situ* instrumentation.

## **3.2. Hydrodynamics**

A wide range of *in-situ* instrumentation was deployed for varying durations during the wintertime experiment to monitor the hydrodynamic conditions from the lower reach of the MR out to about 1 km offshore of the MR mouth. The complete list of instrumentation is found in **Table 1**. Instrument configurations, pairings, and deployment times and locations are described in the sub-sections that follow.

### **3.2.1. Quadpods and ADCP mooring**

Four small quadpods were fabricated for deploying instrumentation suites in the final reach of the MR and the adjacent estuary and sea out to depths of about 7 m. The quadpods are small pyramid shaped structures with an overall height of about 1 m and a roughly square base about 1 m x 1 m. Four large square plates were placed at the four corners of the base to prevent the quadpods from sinking in soft sediments and to provide a location for weights to prevent the quadpods from being disturbed or mobilized by large waves or currents.

Two different instrumentation suites were each deployed on two of the four quadpods with one of each of the two different instrumentation suites deployed in the river and the sea, respectively. The first instrumentation suite (UFQ) included one 1.5 MHz SonTek PC-ADP

(Pulse Coherent Acoustic Doppler Profiler), two Campbell Scientific OBS-3+ (Optical Backscatter) turbidity sensors, one Campbell Scientific OBS-5+ (Optical Backscatter) turbidity sensor, and one MicroCat CT (conductivity and temperature) probe (see photo in **Figure 2a**). The PC-ADP provides the vertical profile of flow velocity and signal strength (acoustic backscatter). The PC-ADP includes a pressure sensor, and can drive and log separate conductivity, temperature and turbidity sensors sampling synchronously with flow measurements. The acoustic and optical backscatter information from the system can be used to estimate the vertical profile of suspended sediment concentration (SSC) (e.g., Sahin et al., 2013). The positions of the instruments with respect to the bed are reported in meters above the bed (mab). A quadpod deployed in the river (at QR1 and QR2) has the PC-ADP mounted at 0.51 mab, OBS-3+ sensors mounted at 0.10 mab and 0.20 mab, OBS-5+ mounted at 0.05 mab, and the MicroCat CT mounted at 0.59 mab. The quadpod deployed in the sea (QS1) has the PC-ADP mounted at 0.54 mab, OBS-3+ sensors mounted at 0.16 mab and 0.26 mab, OBS-5+ mounted at 0.06 mab, and the MicroCat CT mounted at 0.60 mab. Both PC-ADPs were programmed for a 5-cm blanking distance and a bin size of 1.6 cm (35 total bins in the profile). All instruments were logged continuously at 2 Hz.

The second instrumentation suite (NRLQ) deployed on two of the four quadpods included a pair of Nortek HR-Aquadopps with one profiling up mounted at 0.23 mab and one profiling down mounted at 0.54 mab, respectively, to provide a combined vertical profile of flow velocity and signal strength (acoustic backscatter) from the bed up to about 1.30 mab (see photo in **Figure 2b**). Both Aquadopps were programmed with a 10-cm blanking distance, and the up and down profiles had bin sizes of 5 cm and 2 cm, respectively (40 total bins in the combine profile). The Aquadopps include pressure and temperature sensors that logged at 1 Hz. Data was

recorded in bursts for 45 minutes starting at the top of every hour at 2 Hz. Additionally, the second instrumentation suite contained an Imagenex pencil beam sonar operating at a frequency of 1.0 MHz and an Imagenex sector scanning sonar operating at a frequency of 2.25 MHz were used to perform hourly scans of the bed beneath and adjacent to the quadpod. The pencil beam transducer was located 0.40 mab and performed 10 successive line scans each 90° wide. The sector scanning sonar transducer was located 0.51 mab and performed 10 successive 360° rotary scans with 0.3° head angle spacing.

Farthest offshore a Sentinel acoustic Doppler current profiler (ADCP) from Teledyne RDI ® was deployed in about 7 m water depth (see photo in **Figure 2c**). The Sentinel included an upgraded directional wave measurement capability. Hourly observations of wave height and direction and current profiles were recorded.

### **3.2.2. Drifters**

Several riverine drifters (©QinetiQ North America) were launched by hand in the final reach of the MR and recovered using a small boat (see photo in **Figure 2d**). Riverine drifters are spherical in shape having a 0.15 m diameter and weigh less than 1.8 kg. Currents, depth, and temperature are logged onboard the drifter. Location is determined with a standard GPS. Drifters have approximately a 24-hour battery life and are reusable.

### **3.3. Morphodynamics**

Changes in bathymetry were quantified with a series of multibeam surveys performed in the lower reach of the MR and the adjacent estuary. Surveys were performed using an ODOM ES3 operating at 240 kHz with an integrated GPS and inertial measurement unit (IMU). The system used 90 beams with a 1.5° spacing. The investigation area of the transducer was about a 120° linear swath having a width greater than 4 times the depth. The system accuracy was

< 3 cm RMS. Due to the high repetition rate of transmit transducer, surveys were performed at speeds of more than 6 knots. The acquisition of multibeam and navigation data was performed using the HYPACK ® software.

### **3.4. Water column profiles and discrete sampling**

A hand-deployed, Hach Quanta Hydrolab ® was deployed at regular intervals from a small boat both in the river and the estuary to log vertical profiles of temperature, pH, salinity, and turbidity. Surficial sediments were collected using a hand-deployed mini-Ponar grab sampler and short sediment cores were obtained from the river and estuary using a custom made, hand-deployed, messenger tripped gravity core. Water samples containing flocculated sediments were bottled and brought back to the laboratory for particle size analysis using a CILAS 1190 Particle Size Analyzer (PSA)®. While transporting cohesive sediments to the laboratory for analysis is a common practice, alteration of the cohesive sediment properties is likely to occur. In situ quantification of floc size and shape, e.g. using in situ imaging systems, like INSSEV (Fennessy et al., 1994) or LISST (Sequoia Scientific Inc.) is preferred, as demonstrated by several studies during which video systems have been extensively used to measure floc size and settling velocity, in order to both understand the floc dynamics and calibrate theoretical/numerical models (e.g., Winterwerp et al., 2006; Manning and Dyer, 2007; Manning and Schoellhamer, 2013; Soulsby et al., 2013). To better estimate the floc characteristics, future surveys of the MR estuary will include both in situ (direct floc size and settling velocity population measurement) and laboratory investigations.

## **4. Results**

The measurements obtained during the wintertime field experiment provide an overview of the complex dynamics governing the flux of sediment at the mouth and estuary of the MR.

The majority of the *in-situ* instrumentation was deployed and recovered during the period from 20-31 January 2014. A Bora storm occurred during 24-25 January 2014 with *in-situ* instrumentation recording at location QR2 (two pods deployed here contemporary) in the final reach of the river and QS1, QS2, and QS3 in the sea just offshore of the river mouth and estuary (**Figure 1a**). The operation times for each of the four quadpods and the offshore ADCP (located at QS3) are summarized in **Table 2**. The results obtained from the various instrumentation packages described above are systematically presented here with limited discussion. A detailed discussion and comparison of the wintertime and summertime observations are made below, in Section 5.

#### **4.1. Meteorology**

During the period from 20 January – 4 February 2014, the most frequent wind came from NW (17.8%) and WNW sectors (17.4%), followed by SE direction (17.1%). The most intense wind speed was measured from the NE during the storm of 24-25 January 2014. During this event, which lasted 28 hours, the wind direction was almost constant at about 22.5°N. The mean wind speed over the period was of  $11.3 \text{ m s}^{-1}$ , while the maximum of mean speeds and the peak speed were  $18.8 \text{ m s}^{-1}$  and  $25.0 \text{ m s}^{-1}$ , respectively. An intense, but shorter, event was observed on 21 January 2014, with the wind coming from 315°N (NW) and characterized by a mean wind speed of  $10.0 \text{ m s}^{-1}$ . The local rain data confirmed that the storm events of 21 and 24-25 January 2014 were characterized by an intense precipitation in terms of both total daily rain and rain rate.

#### **4.2. Hydrodynamics**

The hourly and daily hydrodynamic conditions in the final reach of the MR are strongly influenced by a combination of precipitation, tides, winds, and waves. During the wintertime experiment, the interplay between these forces strongly modulated the discharge into the sea. In

the summertime, conditions were more benign with low discharge, small waves, and changing winds. The hydrodynamic conditions during the wintertime experiment were characterized with a suite of instrumentation at a number of different locations described below.

#### **4.2.1. Drifters**

The river surface flow in the final reach of the MR was the dominant forcing in the wintertime experiment. The surface drifters were launched more than one hundred times during the campaign to measure speed, direction and temperature. The tracks have been divided into three different strokes (or paths) referring to: (1) the river portion upstream of the bend, (2) the river portion downstream of the bend, and (3) the area outside the estuary. The mean speed and direction for drifter observations obtained during the wintertime experiment in each of the three strokes are compiled in **Table 3**. The speed increased downstream of the bend (passing from stroke 1 to 2) and was greatest in the sea (stroke 3). The direction of the drifters was always consistent with the MR orientation ( $\sim 10\text{-}30^\circ\text{N}$ ), and the drifters followed the MR plume into the sea. The drifter tracks suggested that on average the river surface flow was dominant over the influence of tides and waves.

#### **4.2.2. Current profiles**

During the wintertime experiment three of the four quadpods were deployed at three different locations at different times along the final reach of the MR (**Table 2**). Two quadpods were deployed at QR1 from the period starting at 1030 on 22 January 2014 through 0930 on 24 January 2014. The two quadpods were recovered just past 0930 on 24 January 2014 and deployed again at QR2 starting at 1015 on 24 January 2014 through 0910 on 29 January 2014. Additionally, a third quadpod was deployed at QR3 starting at 1400 on 27 January 2014 through 0910 on 29 January 2014.



Profiles of mean currents and direction observed at QR1, QR2, and QR3 for NRLQ (45-minute burst averaged) are shown in **Figure 3**, **Figure 4**, and **Figure 5**, respectively. In all cases mean currents are plotted in the upper panels and directions of mean currents are plotted in the middle panels. The observed directions exhibited a significant amount of variance. The observed variance in direction was persistent regardless of measurement correlation values. Some of the observed variance may have been due to the uncertain location of the instruments across the width of the channel coupled with secondary flows from the buoyant river plume and the slight bend in the channel at QR3. Additionally, some of the variance with respect to the NRLQ instruments resulted from the orientation of the quadpod in the flow with Aquadopp sensor heads nominally pointed upstream. Particularly, during times of salt wedge intrusion the Aquadopps were measuring nearbed flow in the wake of the quadpod. The normalized backscatter intensity plotted in the lower panel for all cases along with observed changes in bed elevation will be presented below in Section 4.3.2.

For the majority of the period of observation at QR1 (located 525 m upstream of the river mouth) the current in the lower meter of the water column was nearly stagnant with a small, but measurable upstream component suggesting the presence of a salt wedge near the bed (**Figure 3** – upper). Just before the onset of the storm event during the time from 0930 to 1030 on 24 January 2014, the two quadpods were relocated from QR1 to QR2 (located 400 m upstream of the river mouth). During the Bora storm event from about 1100 on 24 January 2014 until about 2400 on 25 January 2014 we observed flushing of the channel at QR2 (**Figure 4**) evidenced by the strong near bed current profile (upper panels) and the alignment of the flow direction across the entire observed profile (middle panels). Starting around 0000 on 26 January 2014 the magnitude of the strong near bed flow towards the sea reversed direction and decreased to less

than  $0.10 \text{ m s}^{-1}$  similar to the conditions prior to the storm indicating the return of the salt wedge in the lower meter of the water column. However, the near  $180^\circ$  change in direction across the lower water column (**Figure 4** – middle) suggested that the salt wedge appeared to be confined to a range between 0.8 – 1.2 mab. Above the salt wedge the buoyant river plume flowed towards the sea with a speeds up to  $0.4 \text{ m s}^{-1}$  between 1.0 – 1.2 mab (**Figure 4** – upper). The small, upstream directed current very near the bed ( $< 0.5$  mab) persisted until a second storm occurred on 28 January 2014. During the second, smaller storm we observed the flow direction towards the sea across the entire lower water column for just a brief time period starting around 1200 until about 1800 on 28 January 2014 at QR2 (**Figure 4**). Additionally, during the second smaller storm there was a third quadpod with instrumentation suite NRLQ located at QR3 (280 m upstream of the river mouth). At the location QR3 flow reversal towards the sea was not observed (**Figure 5** - middle) suggesting the existence of a convergence zone between QR2 and QR3.

During the wintertime experiment two of the four quadpods were deployed at two different locations in the sea (**Table 2**). One quadpod with instrumentation suite UFQ was deployed at QS1 in about 5 m water depth from the period starting at 0930 on 23 January 2014 through 1220 on 27 January 2014. Another quadpod with instrumentation suite NRLQ was deployed at QS2 in about 6 m water depth from the period starting at 1000 on 23 January 2014 through 1200 on 27 January 2014. The observations at QS1 and QS2 spanned the Bora storm of 24-25 January. Profiles of mean currents, direction, and backscatter intensity observed at QS1 and QS2 for UFQ (20-minute averaged) and NRLQ (45-minute burst averaged) are shown in **Figure 6** and **Figure 7**, respectively. Mean currents near the bed ( $< 0.5$  mab) at QS1 prior to the arrival of the storm were typically much less than  $0.2 \text{ m s}^{-1}$  with directions varied (**Figure 6**).

During the hours of 1200 on 24 January through 0000 on 25 January 2014 the currents near the bed roughly aligned directed alongshore to the south and began increasing in magnitude and eventually peaked at over  $0.8 \text{ m s}^{-1}$  very near the bed ( $< 0.5 \text{ mab}$ ). Similarly, mean currents near the bed ( $< 1.2 \text{ mab}$ ) at QS2 prior to the arrival of the storm were typically much less than  $0.2 \text{ m s}^{-1}$  with directions varied (**Figure 7**). During the hours of 1200 on 24 January through 0000 on 25 January 2014 the currents near the bed roughly aligned directed alongshore and began increasing in magnitude and eventually peaked near  $0.80 \text{ m s}^{-1}$ . After the passage of the storm, starting around 0000 on 26 January 2014, the mean currents near the bed ( $< 1.2 \text{ mab}$ ) at QS2 exhibited similar conditions to those observed before the storm. Observed changes in backscatter intensity and local bed elevation will be presented below.

### **4.3. Morphodynamics**

The overall morphodynamics picture was best captured by a series of bathymetric surveys that were obtained around the summertime experiment in May and September 2013 (Brocchini et al., 2015) and after the wintertime experiment in February 2014. Additionally, evidence of sediment transport and short term changes in bed elevation were observed at various quadpod locations during the storms of 24-25 January and 28 January 2014. Observed local changes will be presented below.

#### **4.3.1. Bathymetric surveys**

Bathymetry was obtained from a multibeam survey after the wintertime experiment in February 2014 in the final reach of the MR extending from just upstream of QR1 out past the river mouth and estuary region. The wintertime bathymetry was compared with the bathymetry obtained using the same multibeam system at the end of the summertime experiment in September 2013. Shown in **Figure 8a** and **8b** are the bathymetric surveys for September 2013

and February 2014, respectively. There was up to 1 m of erosion in the channel along the reach from QR1 to QR3 as evidenced in the bathymetry difference plot for the time period between September 2013 and February 2014 (**Figure 8d**). In the final reach from QR3 extending to the river mouth there was very little change in the bathymetry until reaching the end of the channel. At the end of the engineered river channel and just beyond the channel to the south an alternating pattern of deposition and erosion was evident with the erosion and deposition beyond the channel suggesting the formation of a nearshore bar system. Just beyond the channel to the north was a large region of deposition.

#### **4.3.2. Sediment transport**

Periods of intense sediment transport during the wintertime experiment were inferred from variations in the observed backscatter intensity at quadpod locations QR2, QR3, QS1, and QS2. Time series of the vertical profiles for the normalized backscatter intensity were plotted in lower panels of **Figures 3-7**. Here we simply normalized the observed backscatter intensity by the maximum for the time series record at each location (i.e., normalization is different for each Figure). We also observed that increases in backscatter intensity often coincided with observed changes in local bed elevation. Consequently, it was assumed that increased sediment load was likely the main factor driving observed increases in backscatter intensity.

The NRLQ also contained a pencil beam sonar (1 MHz), which effectively was deployed as an acoustic altimeter. The pencil beam sonar performed a series of 10 successive line scans (90° width) every hour. The line scans were averaged to obtain a single distance from the transducer to the bottom once an hour. The location of the bed as determined by the pencil beam sonar is overlaid on all panels of **Figure 3, Figure 4, Figure 5, and Figure 7**. In **Figure 6**, the

location of the bed as determined by the backscatter intensity from the PC-ADP is overlaid on all panels.

During the storm from 24-25 January 2014, backscatter intensity peaked at QR2 near the bed (**Figure 4** – lower). The vertical location of the peak in backscatter intensity during the storm remained close to the bed ( $< 0.5$  mab) at QR2 and was observed to reduce afterwards. The appearance of a rise in bed elevation immediately upon deployment, probably due to local deposition or pod sinking, and then gradual decay starting from 1100 until about 2200 on 24 January 2014 at QR2 was evident (**Figure 4**). At QS1 (**Figure 6**) and QS2 (**Figure 7**) similar peaks in backscatter intensity were observed during the storm on 24-25 January 2014. The backscatter intensity began growing around 0700 on 24 January 2014. At QS1 a gradual deposition ( $< 0.1$  m) from 1200 on 24 January through 0000 on 25 January 2014. The gradual deposition was followed by rapid deposition from 0000 through about 0600 on 25 January 2014 that eventually saturated the signal as the freshly deposited bed approached the transducers of the PC-ADP. Nearly 0.5 m of sediment were deposited at QS1 during the storm and remained in place over the quadpod until the recovery on the morning of 27 January 2014 (**Figure 6**). Similarly, at QS2, rapid deposition occurred from 0000 through about 0600 on 25 January 2014. Subsequently the rate of deposition slowed and subsided around 1800 on 25 January 2014. Roughly 0.2 m of sediment were deposited at QS2 during the storm and remained in place over the quadpod until the recovery on the morning of 27 January 2014 (**Figure 7**).

During the storm on 28 January 2014 the backscatter intensity peaked again and small, but consistent changes in bed elevation were observed at QR2 (**Figure 4**). The conditions during the storm on 28 January 2014 were quite different at QR3 located just 120 m downstream of QR2 where up to 0.4 m of sediment deposition was observed (**Figure 5**). The pencil beam sonar

was completely saturated as deposition began around 0600 and completely covered the sonar by 1000 on 28 January. The sonar head remained buried until after the storm subsided on the morning of 29 January. Strong currents up to  $0.4 \text{ m s}^{-1}$  (**Figure 5** – upper) were observed roughly between 1200 and 1800 on 28 January, but were directed upstream (**Figure 5** – middle) suggesting the source of the observed deposition was from the convergence of downriver transport and waves and currents transporting sediment from the mouth up the channel.

#### **4.4. Water and Sediment Samples**

Water column profile data and discrete water and sediment samples were collected throughout the final reach of the river, the estuary and the nearshore area in front of it, with the aim to investigate the role of wintertime conditions in the estuarine dynamics. Large plumes of sediment were visually observed in the area during and after the storm events on 24-25 January and 28 January 2014. Efforts were made to obtain water and sediment samples during quiescent conditions following each of the storms with small boats.

##### **4.4.1. Water column profiles**

Analyses of water column profiles suggested that precipitation and tides significantly influenced the temperature and salinity of the lower reach of the MR, dramatically changing the estuarine circulation and mixing. However, the observed pH was almost constant along the water column and throughout the investigated period. Due to an increased supply of eroded basin materials, an increase in river turbidity was observed during high-flow states. Further, the MR under normal conditions resembled a partially-mixed estuary but under higher river flow conditions the lower reaches of the MR took on the characteristics of a salt-wedge estuary, with a clear stratification between the fresh surface waters flowing seaward and more saline bottom waters flowing landward.

#### 4.4.2. Riverbed sediment samples

Riverbed sediments were collected primarily in the final 620 m of the MR (i.e., between the train bridge and the mouth). It was observed that sediments were highly heterogeneous, with a mix of gravel, mud and sand within this transitional zone of the MR. In particular, the central portion of the river was characterized by large concentrations of gravel, due to surficial deposits, while in some spots of this zone sample coring was prevented, due to a large concentration of particulate organic matter, comprised of grasses, twigs and leaves. The photographs in **Figure 9** depict material that was freshly deposited on the quadpod located at QR3. A dense mixed layer of fine-grained sediments and organic material remained on the base of the quadpod during the recovery process. The inset (**Figure 9**) is a photograph of material from a diver grab sample that was recovered at QR1 prior to the storm of 24-25 January 2014. The similarity of sediment samples before and after the storm demonstrated that the dense layer of fine-grained sediments and organic material was persistent along the final reach of the MR and throughout the experimental period. The deposits suggested a protective top layer of the river bed that may act as a mat of organic matter that inhibits short-term erosion of the bed.

The fine-grained sediment fraction was characterized by clay and siliceous minerals, with montmorillonite dominating the clay mineralogy. Montmorillonite tends to form large aggregate flocs, which settle rapidly within the estuary during low flow, and which shear apart during the turbulent flows of winter, into small flocs, which are transported in suspension within the plume. In the interim periods, such as during slack tides or other periods of reduced stress it is likely that flocs could aggregate into larger sized flocs. The mineralogy was consistent throughout the final reach of the MR (fine-silt and clay-sized sediment deposits) with fine-grained sediment and silt dominant, except in the area around the train bridge and the adjacent 50-70 m downstream,

where sandy gravel lag-deposits dominated the middle of the river bed. At the river mouth, the grain size distribution switched to fine-sand, which characterized the nearshore littoral up to the offshore quadpods and the “plume” area. Hence, in this region the sediment was dominated by fine-grained quartz sands, with clay- and silt-sized sediments comprising a small fraction of the seafloor sediment assemblage. The observed provinces of sediment suggested that clays are concentrated within the river and widely dispersed outside the river mouth, under the plume and within the nearshore zone.

#### **4.4.3. Suspended sediment samples and flocculated particles**

Suspended sediments were collected in the water column and analyzed. As observed from the surface-water analyses, they were found up to the plume edge (~1.3 km offshore of the river mouth) with the fine sand dominating the sediment size distribution. A large portion of the suspended matter collected within the MR was characterized by flocculated sediments. Flocculated particles in suspension displayed a potential to decrease size and disaggregate as flow velocities were increased. Comparing the response of flocs sampled at the same locations (see **Table 4**), we observed that after the passage of the storm on 24 – 25 January 2014 the sizes of the natant flocs were larger on 26 January than on 27 January 2014. However, the sizes of the natant flocs sampled on 29 January 2014, after the passage of the next storm on 28 January 2014, were more comparable to the smaller flocs collected on 27 January 2014. While flocs tend to disaggregate under higher shear stresses (e.g., during the peak of the storm), they also tend to strongly aggregate when the storm subsides, during the transition from high to low flow conditions. Both the duration and magnitude of the storm on 28 January were less than the storm on 24 – 25 January 2014. The observation of only the smaller flocs remaining in the water column on 29 January 2014 suggested that any larger flocs formed while the storm subsided had



already been deposited when the sampling occurred. While we believe flocc deposition was also the cause for the reduction in size of the natant flocs between 26 and 27 January 2014, the need for in situ measurements of flocc size distributions (e.g., using INSSEV or LISST instruments) within the river plume would greatly increase our understanding about the segregation and distribution of macro- and micro-flocs.

## **5. Discussion**

The results of the wintertime experiment presented above showed significant differences from the summertime experiment (Brocchini et al., 2015) across all the investigated fields including the meteorology (wind and rainfall), the hydrodynamics observed both in the sea and in the river (surface flow and current profiles), and the morphodynamics (bathymetric changes and sediment characteristics). The primary differences were found in the wind forcing, which generated waves of moderate/large heights during the summertime/wintertime, essentially due to the more/less frequent changes in direction, rather than in the velocity. Further, waves generated in winter by WNW, N or NNE (Bora) winds can easily enter the river mouth, as after a small refraction they are almost perfectly aligned to the river direction. Other winds coming from ESE (Scirocco), generated waves which even after the seabed refraction, were still too angled to easily enter the river channel. The Scirocco-generated waves probably more strongly affected the morphology around the estuary, being partially reflected by the river walls.

During wintertime storm events there is an enhanced transport of sediments that influences the morphological and rheological properties of the bed in the vicinity of the river mouth and in the area under the river plume. The suspended sediment plume affects the hydrodynamics, increasing the fluid density and viscosity, as evidenced by the observed dampening of capillary waves at the perimeter of the plume. In summertime the flow at the

estuary is ruled by both river and sea forcing, the salt wedge modulated by the tide being evident throughout the experiment. Similarly, the wintertime response of the estuary follows both river and sea forcing during low-flow states, but severe storms/rainfalls caused the river forcing upstream of the bend (290 m from the mouth) to be dominant regardless of tidal oscillations and waves entering the channel. However, downstream of the bend (final 290m), the interaction between sea and river fluxes was important, leading to the observed sediment deposition at that location.

### 5.1. Wintertime versus Summertime

We begin the comparison between wintertime and summertime conditions with the meteorological data recorded during the experiments. **Figure 10** illustrates the observed wind and wave conditions during the summertime experiment in September 2013. The time series shown was partially reconstructed using a north Adriatic implementation of the Coupled Ocean-Atmosphere-Wave-Sediment Transport (COAWST) system (Russo et al., 2013). Both wind and wave directions suggested large variability with the largest significant wave height,  $H_s \approx 1$  m. Conversely, the wind and wave climate during the wintertime experiment (**Figure 11**) was completely extracted from in-situ observations, either local (e.g., using both weather station and offshore ADCP located at QS3) or from the nearby Ancona harbor (~40 km south of Senigallia). The time series was mainly characterized by long periods of almost constant wind and wave directions, which contained the most severe storms with the largest wave heights. In particular, the most severe storm during the experiment was coincident with a long-lasting wind coming from NNE (see the third panel of **Figure 11** between 24-25 January), whose velocity gradually increased until 0000 on 25 January. The second storm occurring on 28 January contained less energy primarily resulting from a smaller wind velocity (fourth panel of **Figure 11**) and a WNW

incoming wind (third panel of **Figure 11**), which forced the waves to be refracted and rotate of about 90°, thus providing wave energy dissipation.

The large influence of both river and sea forcing during the summertime experiment was also supported by the surface flow results (see **Table 5** and **Figure 12**). Surprisingly, the influence wave forcing and tides were comparable to the river discharge and changed the surface flow (e.g., also Brocchini et al., 2015). Some drifter tracks were observed to flow upstream during the summertime (see bottom, left panel, **Figure 12**). Overall, the speeds along individual drifter tracks were reduced in the summertime as compared to the wintertime (top panels, **Figure 12**). On average the flow was slowed down at the bend and decreased at stroke 2, due to both geometry of the MR cross-section and the influence of waves and tides. The influence of the wave forcing was evident in the observed change in direction of the drifters to NW upon exiting the MR in front of the estuary during the summertime as compared to the wintertime (bottom panels, **Figure 12**). Further, while wintertime tracks were always consistent with the streamwise river alignment, with an increasing velocity moving downstream, the importance of the sea forcing on the summertime surface flow was suggested by the larger standard deviations of both speed and direction (**Table 5**). **Figure 12** also shows that longer downriver paths were recorded during wintertime.

When comparing the river current profiles, the main differences are found in the storm events, which affect the wintertime behavior of the estuary, more than the normal-flow conditions. As described in 4.2.2, the storm events forced the flow downstream across the water column in portions of the lower reach of the MR, without any visible influence of the sea forcing upstream of the river bend. However, the flow was significantly influenced by the incoming waves downstream of the bend, suggesting complex dynamics and interactions within the estuary

during storms. The analysis of both the velocity profiles demonstrated that direction was not clearly seaward throughout the lower reach of the MR leading to the observed deposition at QR3 near the bend. Similar deposition was observed at QR2 reaching an initial maximum around 1200 on 28 January, but then was immediately eroded when the flow aligned downstream across the profile. Subsequently, the deposition returned when the flow reversed again near the end of the day on 28 January (**Figure 4**). The observations suggested the generation of sediment trapping (e.g., see Liu et al., 2011) at the bend, or more downstream, due to the convergence of both hydrodynamic fluxes and suspended sediments.

Large sediment transport directed upstream close to the bed with fresh water flowing overtop in the downstream direction has been previously observed (e.g., Traykovski et al., 2004). Similar morphodynamics may explain the large erosion that occurred in wintertime upstream of the bend, where the flow was dominated by the river discharge, and the more complex patterns downstream of the bend and at the mouth, where sediment deposition was also observed (**Figure 8d**). The wintertime morphodynamics were in contrast to the observations from summertime (see also Brocchini et al., 2015), when a large sediment deposition occurred throughout the final reach of the MR, suggesting that the flocculation zone was probably located upstream of the train bridge (**Figure 8c**).

Floc aggregation and transport were significantly affected by the wintertime varying flow conditions, which determined large variations in their size and settling velocity. They were also characterized by mixed fine-grained sediments, hence their properties depended on the percentage of suspended material (e.g., Manning et al., 2010). Further, they were subject to both physical and biological cohesion, as suggested by the large amount of organic matter both

floating at the water surface and deposited on the river quadpod (Figure 9), this also explaining the reduced change of the bed morphology during storms (e.g., Parsons et al., 2016).

## **5.2. Role of waves**

Summertime and wintertime storms were characterized by different atmospheric conditions (see **Figure 10** and **Figure 11**) resulting in distinct wave climates. The direction and intensity of winds was the controlling factor determining the differences in the direction of the incoming waves and the intensity of the storms. The effects of waves on the shoreline and river may be simplified by decomposing the wave energy into two categories. First, swell energy was likely responsible for sediment transport in the estuary, and second, infragravity (IG) wave energy was likely responsible for altering sedimentary processes farther upstream.

Wintertime conditions were dominated by strong sustained northerly winds (blowing along the short axis of the Adriatic) that can reach speeds up to  $20 \text{ m s}^{-1}$ . The relatively short fetch of these winds generated short, steep swells propagating almost shore-normal to the shoreline, and directly into the MR mouth. These short, steep swells generated intense breaking before and at the river mouth, suspending sediment and enhancing sediment transport, as evidenced by the large sediment deposition observed at our offshore quadpods in 5 m (QS1) and 6 m (QS2) water depth during the Bora storm of 25 January. During both observed storms, large wave heights were measured at location QR2, suggesting that only storm conditions are capable of driving pulse-like waves up the channel.

The conditions for the typical summertime storm are driven by south-easterly winds availing themselves of the long fetch of the Adriatic long axis. Summertime storms produce long, narrow-spectrum, but comparatively weaker, less-steep swells that approach the coast with a wide incidence angle. The summertime storms are more efficient producers of IG waves, due

to a longer shallow-water run and less intense breaking. Consequently, the river is more typically affected at larger distances from the river mouth during the summertime, as evidenced by previous surface flow measurements (Section 4.2.1) and salinity values, which were larger than zero up to about 1.8 km upstream and larger than 10 psu between the train bridge and the estuary (Brocchini et al., 2015). Similar summertime dynamics are observed in different rivers where the dry-season enhances prolonged sea water intrusion (Dong et al., 2004).

The combined observations of waves and morphodynamics in the final reach of the MR during wintertime storms were in agreement with the proposed role of storm waves as a fundamental agent for the upstream, nearbed advection of thick layers of fluid mud (e.g., McAnally et al., 2007). We believe that the ~0.4 m of sediment deposition observed at QR3 (**Figure 5**) resulted from the convergence of downstream sediment transport and an upstream, nearbed advection of sediment induced by storm waves.

### **5.3. Comparison with existing studies**

Seasonal variability of estuarine environments has been studied previously, though typically these estuaries have been much larger in size and subject to larger tidal excursions than the MR. While these larger rivers, e.g., the Pearl River, China (Dong et al., 2004), or the Ba Lat River, Vietnam (van Maren and Hoekstra, 2004), are characterized by larger discharges they still exhibit fresh water dominating in the upper layer and salt water intruding landward near the bottom, similar to the conditions in the MR. Despite the large range in size, discharge, and tidal excursion all these estuary systems (including the MR see Section 4.4.1) exhibit (1) highly stratified water columns with small mixing rates during the rainy season (salt-wedge estuary), and (2) partly stratified water columns during the dry season, with a larger water mixing (partly stratified estuary). The seasonal behavior leads to varying dynamics both inside the estuary and

offshore of the mouth (Chao, 1988; Dong et al., 2004). Numerical simulations underline the important role of tides and winds in water mixing, and their influence on bottom turbulence at the plume location (Pan and Gu, 2016).

Winds exhibit different controls on estuarine dynamics. Wind-generated residual currents in the estuarine system mainly affect fine sediment transport (Narváez and Valle-Levinson, 2008). Intertidal areas influenced by small wind-generated waves, which increase the bed shear stress, generate orbital velocities that may be much more efficient than tidal currents in eroding sediments (Noernberg et al., 2007; Hunt et al., 2015). Similar behavior was observed at the MR estuary, where the tidal forcing had a negligible effect on morphological changes, especially given the strong impact of wave-forcing during storms.

#### **5.4. Limitations and possible improvements**

The present study was characterized by some limitations, mainly due to both the reduced number of bathymetric surveys and the lack of in situ floc measurements. Future experiments on the MR estuary will leverage an existing video-monitoring systems installed at the Senigallia harbour in summer 2015, which is enabling an almost real-time reconstruction of both wave field and bathymetry in the estuarine and coastal area. The continuous remotely sensed data will allow us to better quantify the eroded/deposited sediment volumes, especially during high-flow conditions. Further, the use of novel optical techniques for in situ floc measurements in the future will improve identification and classification of floc size and settling velocity.

#### **6. Conclusions**

The experimental campaigns carried out within the estuarine environment of the Misa River (Senigallia, Italy) provided insight into the complex dynamics occurring during both low-flow and high-flow conditions. The baseline (summertime) experiment of September 2013

suggested a strong interaction of waves, tide and river flow within the final reach of the river and at the estuary, where sea forcing-induced waves and currents traveled up to 1.8 km upstream and promoted flocculation within the river at distances larger than 700 m from the estuary. Infragravity waves generated from southeast (Scirocco) winds propagated energy farthest upstream. Further, the bathymetric surveys confirmed that sediment and flocculation deposition occurred in the final 600-700 m of the river.

The wintertime experiment, carried out in January 2014, was characterized by alternating low and high flow conditions, which influenced the river hydro-morphodynamics in different ways. The low flow conditions of the wintertime highlighted a fairly strong interaction between the sea and river forcing, similar to the observations in summertime. However, in the wintertime the surface flow was constantly directed downstream, highlighting the dominance of the river forcing. Additionally, the high flow conditions of the wintertime played an important role controlling the morphological response of both the river and adjacent nearshore region. The wintertime winds were characterized by almost constant directions for much longer periods than in summertime, enabling waves to reach heights up to three times larger. Larger wave heights, coupled with comparable storm surges and larger river flows, when compared to summertime measurements, lead to complex hydro-morphodynamics within the final reach of the MR. In particular, during storm events, river flow dominated over sea forcing at distances from the river mouth larger than ~300 m, the flow being downstream directed throughout the water column and the riverbed being slightly eroded due to the protective action of a surficial muddy layer, mixed with organic matter. Localized patterns of mud deposition at the river entrance were thought to be the result of downstream sediment transport and upstream, nearbed advection of sediment



induced by storm waves. However, such strong sea-river interactions mainly occurred close to the river mouth, due to the reduced contribution of infragravity waves during Bora winds.

## **7. Acknowledgements**

Financial support from the ONR Global (UK), through the NICOP Research Grant (N62909-13-1-N020) and from the Italian RITMARE Flagship Project (SP3-WP4), a National Research Programme funded by the Italian Ministry of University and Research, are gratefully acknowledged. JC, AHR, EFB were supported under base funding to the Naval Research Laboratory from the Office of Naval Research. The authors would like to thank the following authorities: the Municipality of Senigallia, the Capitaneria di Porto of Senigallia and of Ancona, MARIDIPART La Spezia and MARIFARI Venezia. Acknowledgments go also to: GESTIPOINT (Senigallia), Club Nautico (Senigallia), NOTA srl (Senigallia), Carmar Sub (Ancona), Sena Gallica (Senigallia), METIS S.R.L. (Senigallia). Special thanks go to Dr. P. Paroncini and Mr. A. Coluccelli for their help in the maritime operations, to Mr. O. Favoni for his help in the analysis of the sediments, to Prof. E.S. Malinverni, for the use of a total station, to Mr. M. Trinchera for his continued help in all operations and to all the staff working at the lighthouse of Senigallia. Mr. Coluccelli is also acknowledged for the COAWST setup in the northern Adriatic and its operational management, and the Hydro-Meteo-Clima Service of the Emilia-Romagna Environmental Agency (SIMC-ARPA-EMR, Bologna, Italy) for operationally providing boundary conditions (from AdriaROMS, SWAN Italia and COSMO-I7 forecasts, and Po River discharge measurements) to COAWST.

## 8. References

- Brocchini, M., Calantoni, J., Reed, A.H., Postacchini, M., Lorenzoni, C., Russo, A., Mancinelli, A., Corvaro, S., Moriconi, G., Soldini, L., 2015. Summertime conditions of a muddy estuarine environment: the EsCoSed project contribution. *Water Science & Technology* 71(10), 1451-1457.
- Calliari, L.J., Speranski, N.S., Torronteguy, M., Oliveira, M.B., 2001. The mud banks of Cassino Beach, southern Brazil: characteristics, processes and effects. *Journal of Coastal Research*, ICS 2000 Proceedings, 318-325.
- Camuffo, D., 1984. Analysis of the series of precipitation at Padova, Italy. *Climatic Change* 6(1), 57-77.
- Chao, S.Y., 1988. River-forced estuarine plumes. *Journal of Physical Oceanography*, 18(1), 72-88.
- Doglioni, C., Mongelli, F., Pieri, P., 1994. The Puglia uplift (SE Italy): An anomaly in the foreland of the Apenninic subduction due to buckling of a thick continental lithosphere. *Tectonics* 13(5), 1309–1321.
- Dong, L., Su, J., Wong, L.A., Cao, Z., Chen, J.C., 2004. Seasonal variation and dynamics of the Pearl River plume. *Continental Shelf Research* 24(16), 1761-1777.
- Eisma, D., 1986. Flocculation and de-flocculation of suspended matter in estuaries. *Netherlands Journal of Sea Research*, 20(2-3), 183-199.
- Favali, P., Frugoni, F., Monna, D., Rainone, L., Signanini, P., Smriglio, G., 1995. The 1930 earthquake and the town of Senigallia (Central Italy): an approach to seismic risk evaluation, in: Boschi, E. et al. (Eds.), *Earthquakes in the Past: Multidisciplinary Approaches*, *Annali di Geofisica* XXXVIII (5–6). pp. 679–689.

746 Fennessy, M.J., Dyer, K.R., Huntly, D.A., 1994. INSSEV: an instrument to measure the size and  
 747 settling velocity of flocs in situ. *Marine Geology* 117, 107-117.

748 Fox, J.M., Hill, P.S., Milligan, T.G., Boldrin, A., 2004. Flocculation and sedimentation on the Po  
 749 River Delta. *Marine Geology* 203, 95–107.

750 Horvath, K., Lin, Y. L., Ivančan-Picek, B., 2008. Classification of cyclone tracks over the  
 751 Apennines and the Adriatic Sea. *Monthly Weather Review* 136(6), 2210-2227.

752 Hunt, S., Bryan, K.R., Mullarney, J.C., 2015. The influence of wind and waves on the existence  
 753 of stable intertidal morphology in meso-tidal estuaries. *Geomorphology* 228, 158-174.

754 Kennish, M. J., 1986. Ecology of Estuaries. Volume I: Physical and Chemical Aspects, CRC  
 755 Press, Boca Raton, FL.

756 Liu, G.F., Zhu, J.R., Wang, Y.Y., Wu, H., Wu, J.X., 2011. Tripod measured residual currents  
 757 and sediment flux: Impacts on the silting of the Deepwater Navigation Channel in the  
 758 Changjiang Estuary. *Estuarine Coastal and Shelf Science* 93(3), 192-201.

759 Malarkey, J., Baas, J.H., Hope, J.A., Aspden, R.J., Parsons, D.R., Peakall, J., Paterson, D.M.,  
 760 Schindler, R.J., Ye, L., Lichtman, I.D., Bass, S.J., Davies, A.G., Manning, A.J., Thorne,  
 761 P.D., 2015. The pervasive role of biological cohesion in bedform development. *Nature*  
 762 *Communications*, DOI: 10.1038/ncomms7257.

763 Manning, A.J., 2004. Observations of the properties of flocculated cohesive sediment in three  
 764 western European estuaries. *Journal of Coastal Research* SI 41, 70-81.

765 Manning, A.J., Baugh, J.V., Spearman, J.R., Pidduck, E.L., and Whitehouse, R.J., 2011. The  
 766 settling dynamics of flocculating mud-sand mixtures: Part 1 - Empirical algorithm  
 767 development. *Ocean Dynamics*, 61(2-3), 311-350.

768 Manning, A.J., Baugh, J.V., Spearman, J.R., and Whitehouse, R.J., 2010. Flocculation settling  
769 characteristics of mud: sand mixtures. *Ocean dynamics*, 60(2), 237-253.

770 Manning, A.J., and Dyer, K.R., 2002. The use of optics for the in situ determination of  
771 flocculated mud characteristics. *Journal of Optics A: Pure and Applied Optics*, 4(4), S71.

772 Manning, A.J., and Dyer, K.R., 2007. Mass settling flux of fine sediments in Northern European  
773 estuaries: measurements and predictions. *Marine Geology*, 245(1), 107-122.

774 Manning, A.J., and Schoellhamer, D.H., 2013. Factors controlling floc settling velocity along a  
775 longitudinal estuarine transect. *Marine Geology*, 345, 266-280.

776 Manning, A.J., Spearman, J.R., Whitehouse, R.J.S., Pidduck, E.L., Baugh, J.V. and Spencer,  
777 K.L., 2013. Laboratory Assessments of the Flocculation Dynamics of Mixed Mud-Sand  
778 Suspensions. In: Dr. Andrew J. Manning (Ed.), *Sediment Transport Processes and their*  
779 *Modelling Applications*, Publisher: InTech (Rijeka, Croatia), Chapter 6, pp. 119-164, ISBN:  
780 978-953-51-1039-2, DOI: org/10.5772/3401.

781 Mayerle, R., Narayanan, R., Etri, T., Wahab, A.K.A., 2015. A case study of sediment transport in  
782 the Paranagua Estuary Complex in Brazil. *Ocean Engineering* 106, 161-174.

783 McAnally, W.H., Friedrichs, C., Hamilton, D., Hayter, E., Shrestha, P., Rodriguez, H., Sheremet,  
784 A., Teeter, A., 2007. Management of Fluid Mud in Estuaries, Bays, and Lakes. I: Present  
785 State of Understanding on Character and Behavior. *Journal of Hydraulic Engineering*  
786 133(1), 9-22.

787 Mehta, A.J., 2014. *An Introduction to Hydraulics of Fine Sediment Transport*, World Scientific,  
788 Hackensack, N. J.

789 Milligan, T. G., Hill, P. S., Law, B. A., 2007. Flocculation and the loss of sediment from the Po  
790 River plume. *Continental Shelf Research* 27(3-4), 309-321.

791 Milliman, J.D., Syvitski, J.P.M., 1992. Geomorphic/Tectonic control of sediment discharge to  
792 the Ocean: the importance of small mountainous rivers. *The Journal of Geology* 525-544.

793 Narváez, D.A., Valle-Levinson, A., 2008. Transverse structure of wind-driven flow at the  
794 entrance to an estuary: Nansemond River. *Journal of Geophysical Research: Oceans*,  
795 113(C9).

796 Noernberg, M.D.A., Marone, E., Angulo, R.J., 2007. Coastal currents and sediment transport in  
797 Paranaguá estuary complex navigation channel. *Boletim Paranaense de Geociências* 60(61),  
798 45-54.

799 Olsen, C.R., Larsen, I.L., Mulholland, P.J., Vondamm, K.L., Grebmeier, J.M., Schaffner, L.C.,  
800 Diaz, R.J., Nichols, M.M., 1993. The concept of an equilibrium surface-applied to particle  
801 sources and contaminant distributions in estuarine sediments. *Estuaries* 16(3B), 683-696.

802 Pan, J., Gu, Y., 2016. Cruise observation and numerical modeling of turbulent mixing in the  
803 Pearl River estuary in summer. *Continental Shelf Research* 120, 122-138.

804 Parsons, D.R., Schindler, R.J., Hope, J.A., Malarkey, J., Baas, J.H., Peakall, J., Manning, A.J.,  
805 Ye, L., Simmons, S., Paterson, D.M., Aspden, R.J., Bass, S.J., Davies, A.G., Lichtman, I.D.  
806 and Thorne, P.D., 2016. The role of biophysical cohesion on subaqueous bed form size.  
807 *Geophysical Research Letters*, 43, 1566-1573, doi:10.1002/2016GL067667.

808 Rogers, W.E., Holland, K.T., 2009. A study of dissipation of wind-waves by mud at Cassino  
809 Beach, Brazil: Prediction and inversion. *Continental Shelf Research* 29(3), 676-690.

810 Rolandi, G., Paone, A., Di Lascio, M., Stefani, G., 2008. The 79 AD eruption of Somma: The  
811 relationship between the date of the eruption and the southeast tephra dispersion. *Journal of*  
812 *Volcanology and Geothermal Research* 169(1), 87–98.

813 Russo, A., Carniel, S., Benetazzo, A. 2013. Support for ICZM and MSP In the Adriatic Sea  
814 Region Using ROMS Model, COAWST System for Coastal Zone Management. *Sea*  
815 *Technology* 54(8), 27pp.

816 Sahin, C., Safak, I., Hsu, T.J., Sheremet, A. 2013. Observations of suspended sediment  
817 stratification from acoustic backscatter in muddy environments. *Marine Geology* 336, 24-  
818 32.

819 Sanford, L.P., 1992. New sedimentation, resuspension, and burial. *Limnology and Oceanography*  
820 37, 1164-1164.

821 Sanford, L.P., Maa, J.P.Y., 2001. A unified erosion formulation for fine sediments. *Marine*  
822 *Geology* 179(1), 9-23.

823 Schindler, R.J., Parsons, D.R., Ye, L. , Hope, J A., Baas, J.H., Peakall, J., Manning, A. J.,  
824 Aspden, R.J., Malarkey, J., Simmons, S., Paterson, D. M., Lichtman I.D., Davies, A.D.,  
825 Thorne, P.D., and Bass, S.J., 2015. Sticky stuff: Redefining bedform prediction in modern  
826 and ancient environments. *Geology* 43(5), 399-402.

827 Sholkovitz, E.R., 1976. Flocculation of dissolved organic and inorganic matter during the mixing  
828 of river water and seawater. *Geochimica et Cosmochimica Acta* 40(7), 831-845.

829 Smith, J.P., Bullen, T.D., Brabander, D.J., Olsen, C.R., 2009. Strontium isotope record of  
830 seasonal scale variations in sediment sources and accumulation in low-energy, subtidal areas  
831 of the lower Hudson River estuary. *Chemical Geology* 264(1-4), 375-384.

832 Soulsby, R.L., Manning, A.J., Spearman, J., and Whitehouse, R.J.S., 2013. Settling velocity and  
833 mass settling flux of flocculated estuarine sediments. *Marine Geology*, 339, 1-12.

834 Spearman, J.R., Manning, A.J., and Whitehouse, R.J., 2011. The settling dynamics of  
 835 flocculating mud and sand mixtures: Part 2 - Numerical modelling. *Ocean Dynamics*, 61(2-  
 836 3), 351-370.

837 Spencer, K.L., Manning, A.J., Droppo, I.G., Leppard, G.G., and Benson, T., 2010. Dynamic  
 838 interactions between cohesive sediment tracers and natural mud. *Journal of soils and*  
 839 *sediments*, 10(7), 1401-1414.

840 Thorne, P.D., Agrawal, Y.C., and Cacchione, D.A., 2007. A comparison of near-bed acoustic  
 841 backscatter and laser diffraction measurements of suspended sediments. *IEEE Journal of*  
 842 *Oceanic Engineering*, 32(1), 225-235.

843 Thorne, P.D., and Hurther, D., 2014. An overview on the use of backscattered sound for  
 844 measuring suspended particle size and concentration profiles in non-cohesive inorganic  
 845 sediment transport studies. *Continental Shelf Research*, 73, 97-118.

846 Traykovski, P., Geyer, R., Sommerfield, C. 2004. Rapid sediment deposition and fine-scale  
 847 strata formation in the Hudson estuary. *Journal of Geophysical Research - Earth Surface*  
 848 109(F2), F02004.

849 van Maren, D.S., Hoekstra, P., 2004. Seasonal variation of hydrodynamics and sediment  
 850 dynamics in a shallow subtropical estuary: the Ba Lat River, Vietnam. *Estuarine, Coastal*  
 851 *and Shelf Science*, 60(3), 529-540.

852 Whitehouse, R.J.S. and Manning, A.J., 2007. Mixing it: how marine mud and sand interact.  
 853 *Innovation and Research Focus*, Institution of Civil Engineering publishing by Thomas  
 854 Telford Services Ltd (London, UK), 71, pp.2.

855 Whitehouse, R.J.S., Soulsby, R.L., Roberts, W., Mitchener, H.J., 2000. Dynamics of Estuarine  
856 Muds: A manual for practical applications. Thomas Telford, London, ISBN 0-7277-2864-4.

857 Winterwerp, J.C. 2002. On the flocculation and settling velocity of estuarine mud. *Continental*  
858 *Shelf Research* 22(9), 1339-1360.

859 Winterwerp, J.C., Manning, A.J., Martens, C., De Mulder, T., and Vanlede, J., 2006. A heuristic  
860 formula for turbulence-induced flocculation of cohesive sediment. *Estuarine, Coastal and*  
861 *Shelf Science*, 68(1), 195-207.

862 Woodruff, J.D., Geyer, W.R., Sommerfield, C.K., Driscoll, N.W., 2001. Seasonal variation of  
863 sediment deposition in the Hudson River estuary. *Marine Geology* 179(1-2), 105-119.

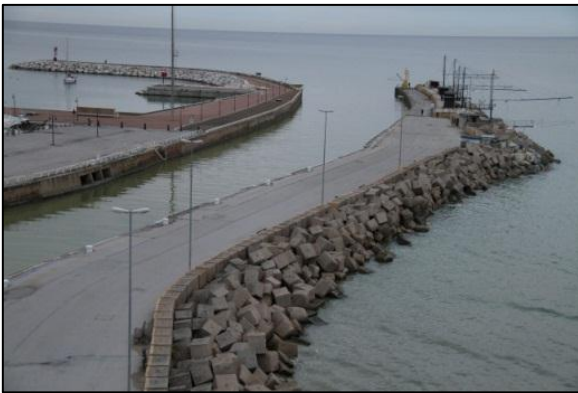
864 Zhu, S., Sheng, J., & Ji, X. (2016). Tidally averaged water and salt transport velocities and their  
865 distributions in the Pearl River Estuary. *Ocean Dynamics* 66(9), 1125-1142.

866





a)



b)



c)

Figure 1 - a) Study area of summer and winter experiments at the MR estuary (Senigallia, Marche Region, Italy), with locations of deployed quadpods in river (QR) and sea (QS). Pictures showing b) the final engineered reach of the MR and c) severe wave conditions at the MR estuary during winter Bora in January 2014.

873

Table 1 - Instrumentation used during wintertime deployment.

Instrument	#	Type	Location	Temporal Resolution
<b>Velocity Profiler</b>	4	Nortek Aquadopp: 2 MHz	QR1	2 Hz for 40 min/hour
			QR2	
			QR3	
			QS2	
<b>Pencil Beam</b>	2	Imagenex 881 A: 600-1000 kHz	QR1	10 line scans per hour
			QR2	
			QR3	
			QS2	
<b>Velocity Profiler</b>	2	Sontek PC-ADP: 1.5 MHz	QR1	2 Hz Cont
			QR2	
			QS1	
<b>CT Probe</b>	2	Seabird MicroCat CT	QR1	2 Hz Cont.
			QR2	
			QS1	
<b>ADCP</b>	1	TRDI Sentinel 1200KHz wave array	QS3	wave hourly

874

875

Table 2 - Operation time of the pods.

Location	Instrument Suite	Operation time [UTC]
<b>QR1</b>	<i>NRLQ</i>	22/01 ( <b>13:30</b> ) to 24/01 ( <b>09:30</b> )
<b>QR1</b>	<i>UFQ</i>	22/01 ( <b>10:30</b> ) to 24/01 ( <b>09:20</b> )
<b>QR2</b>	<i>NRLQ</i>	24/01 ( <b>10:45</b> ) to 29/01 ( <b>09:10</b> )
<b>QR2</b>	<i>UFQ</i>	24/01 ( <b>10:15</b> ) to 29/01 ( <b>09:00</b> )
<b>QR3</b>	<i>NRLQ</i>	27/01 ( <b>14:00</b> ) to 29/01 ( <b>09:30</b> )
<b>QS1</b>	<i>UFQ</i>	23/01 ( <b>09:30</b> ) to 27/01 ( <b>12:20</b> )
<b>QS2</b>	<i>NRLQ</i>	23/01 ( <b>10:00</b> ) to 27/01 ( <b>12:00</b> )
<b>QS3</b>	<i>ADCP</i>	23/01 ( <b>11:10</b> ) to 29/01 ( <b>12:20</b> )

876

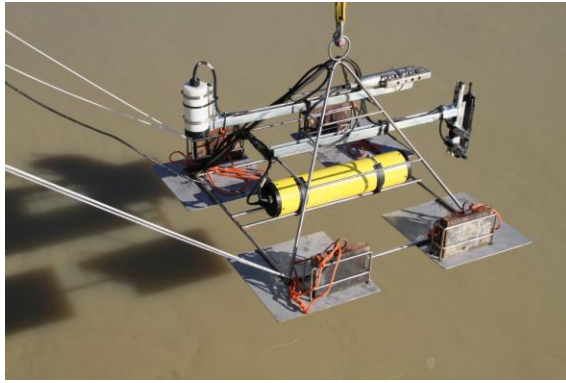


Figure 2 - Quadpods for the measurements of (a) suspended sediments (QR1, QR2, QS1) and (b) flow velocity (QR1, QR2, QR3, QS2); (c) ADCP for measurements of offshore wave characteristics (QS3); (d) surface Lagrangian drifters (river and estuary).

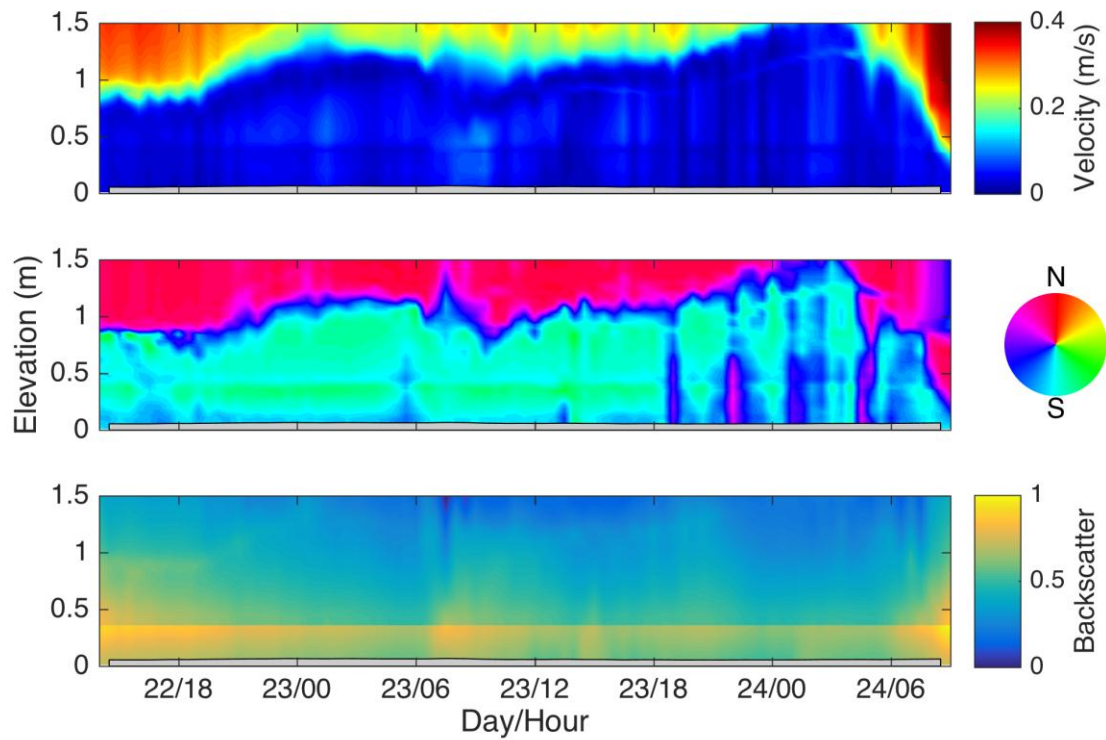
883

Table 3 - Surface flow features recorded by the drifters.

	stroke	Jan 22 <sup>nd</sup>	Jan 23 <sup>rd</sup>	Jan 26 <sup>th</sup>	Jan 27 <sup>th</sup>	Jan 29 <sup>th</sup>
mean speed [m/s]	1	0.329±0.068	0.297±0.059	0.225±0.079	0.364±0.068	0.335±0.088
	2	0.463±0.107	0.360±0.081	0.324±0.111	0.306±0.093	0.439±0.138
	3	0.454±0.153	-	0.556±0.139	0.302±0.088	-
max speed [m/s]	1	0.823	0.741	0.422	0.463	0.622
	2	0.736	0.787	0.633	0.566	0.684
	3	0.808	-	0.715	0.602	-
direction/course [°N]	1	14.65	15.18	13.15	16.15	13.17
	2	30.83	35.65	30.59	29.51	32.99
	3	33.97	-	25.94	23.96	-
temperature [°C]	all	9.8	9.7	6.6	6.1	7.7

884

885



888

889

890

891

892

893

894

Figure 3. Shown is hourly burst averaged velocity profiles (upper), direction (middle) and normalized acoustic backscatter intensity (lower) observed with the down and up looking Aquadopps at QR1. Backscatter was normalized by the maximum backscatter value from the two Aquadopps for time period shown here. Overlaid on all panels is the location of the bed estimated from hourly averages of the pencil beam sonar line scans.



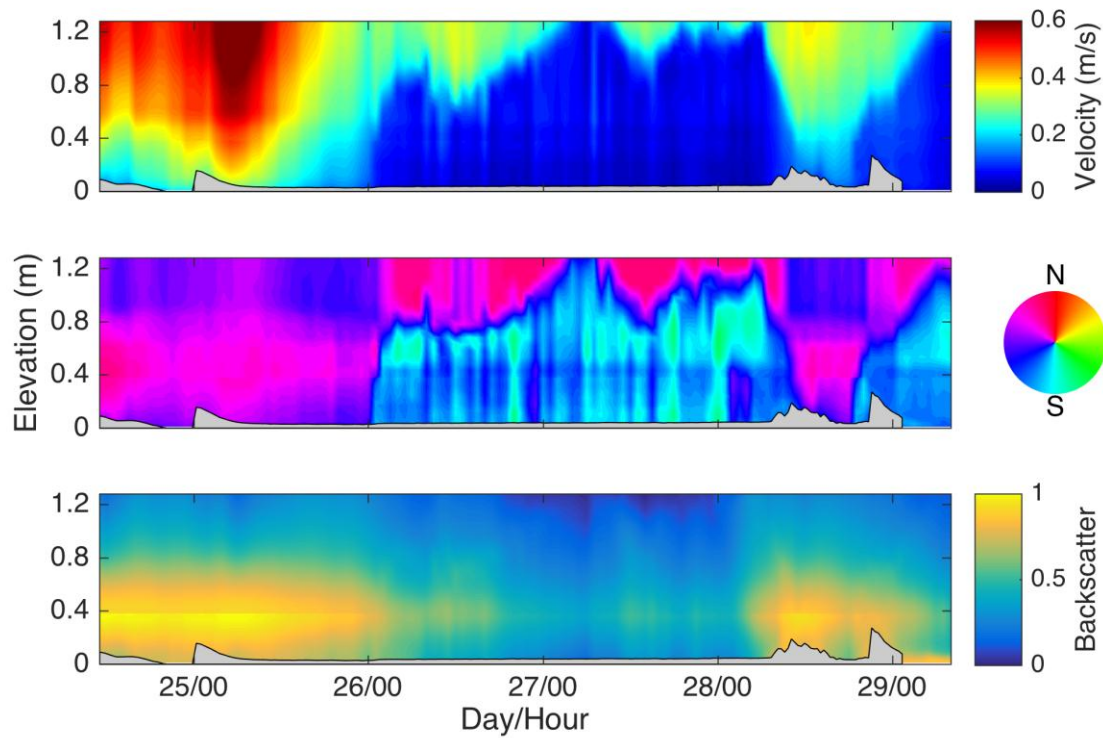


Figure 4. Shown is hourly burst averaged velocity profiles (upper), direction (middle) and normalized acoustic backscatter intensity (lower) observed with the down and up looking Aquadopps at QR2. Backscatter was normalized by the maximum backscatter value from the two Aquadopps for time period shown here. Overlaid on all panels is the location of the bed estimated from hourly averages of the pencil beam sonar line scans.

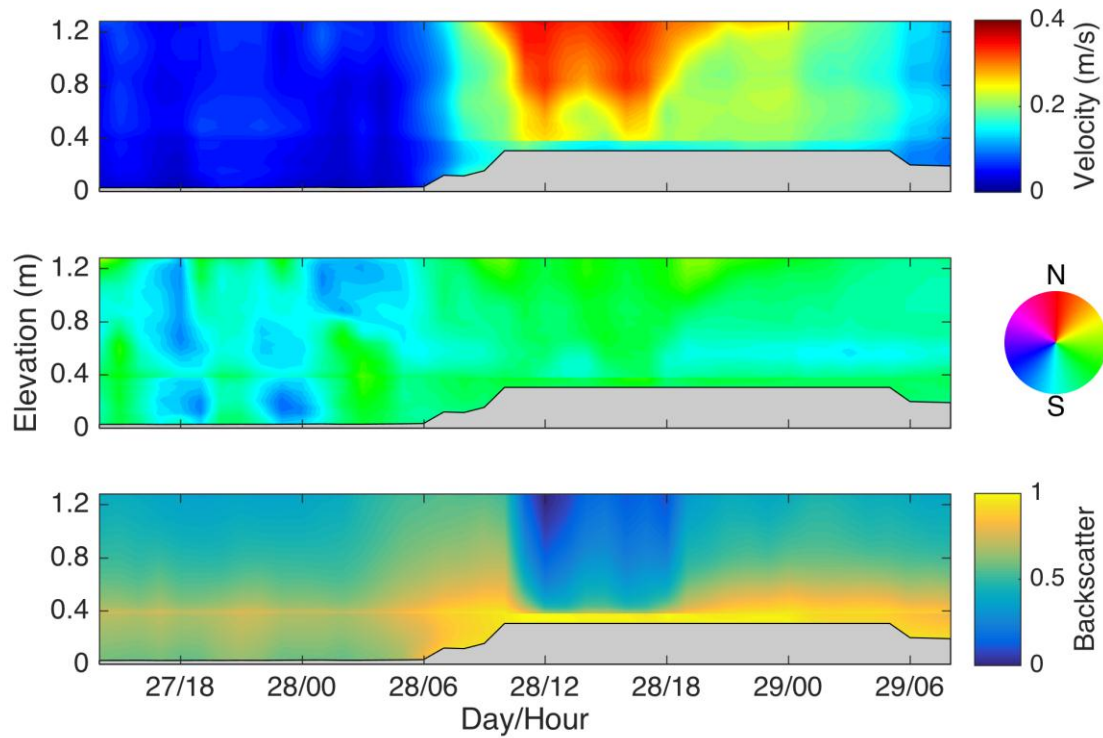


Figure 5. Shown is hourly burst averaged velocity profiles (upper), direction (middle) and normalized acoustic backscatter intensity (lower) observed with the down and up looking Aquadopps at QR3. Backscatter was normalized by the maximum backscatter value from the two Aquadopps for time period shown here. Overlaid on all panels is the location of the bed estimated from hourly averages of the pencil beam sonar line scans.

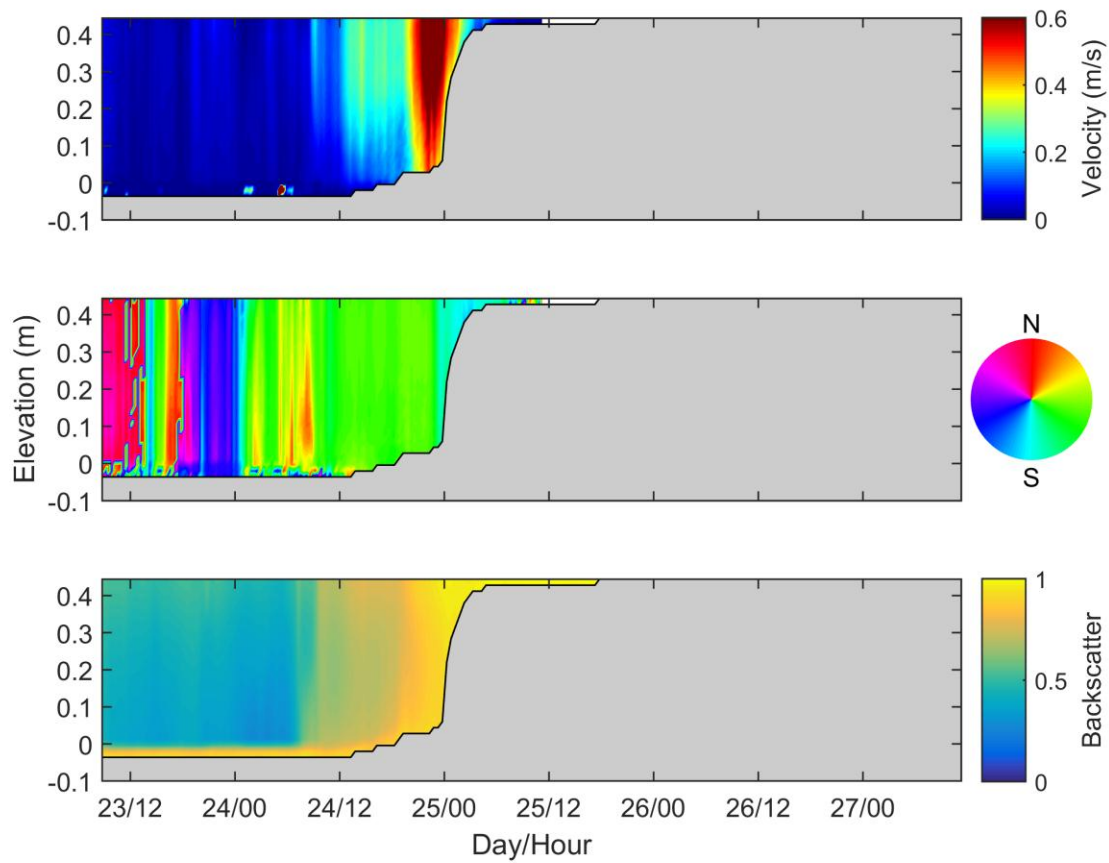


Figure 6. Shown is half hour averaged velocity profiles (upper), direction (middle) and normalized acoustic backscatter intensity (lower) observed with the PC-ADP as QS1. Backscatter was normalized by the maximum backscatter value from the PC-ADP for time period shown here. Overlaid on all panels is the location of the bed estimated using the acoustic backscatter.



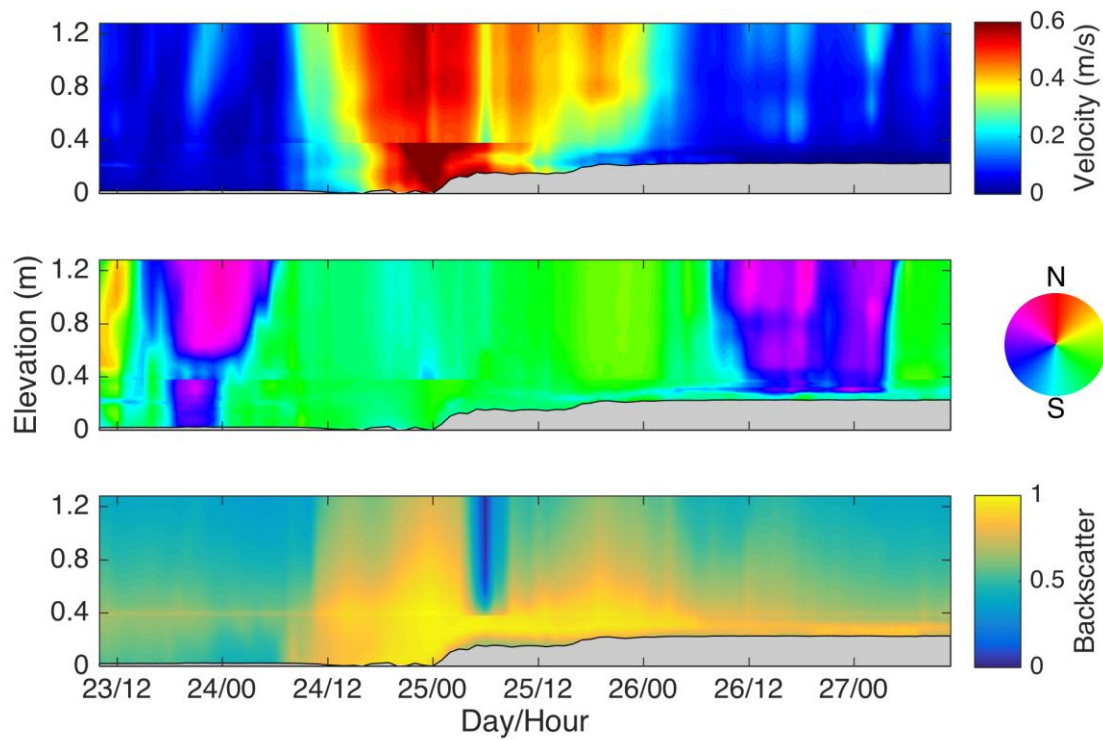
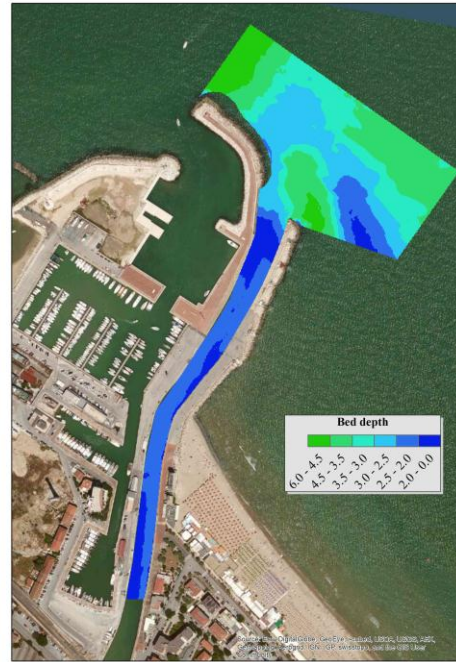


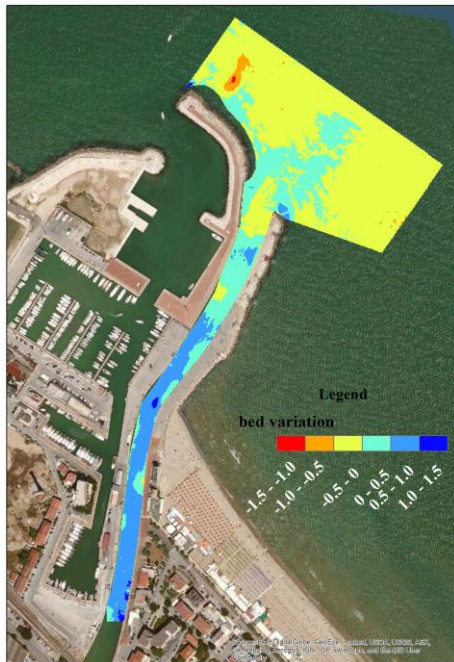
Figure 7. Shown is hourly burst averaged velocity profiles (upper), direction (middle) and normalized acoustic backscatter intensity (lower) observed with the down and up looking Aquadopps at QS2. Backscatter was normalized by the maximum backscatter value from the two Aquadopps for time period shown here. Overlaid on all panels is the location of the bed estimated from hourly averages of the pencil beam sonar line scans.



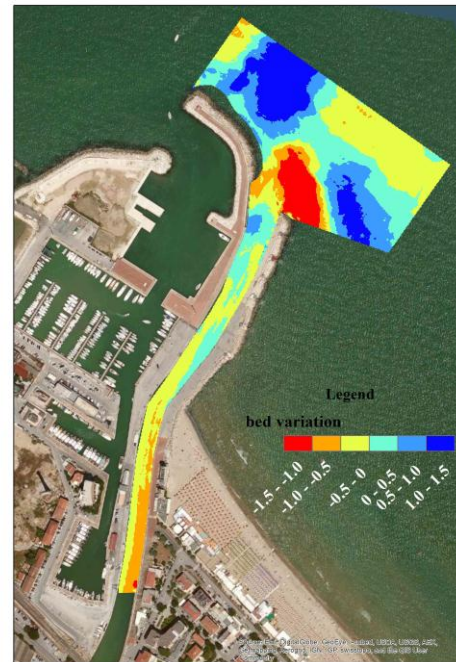
a)



b)

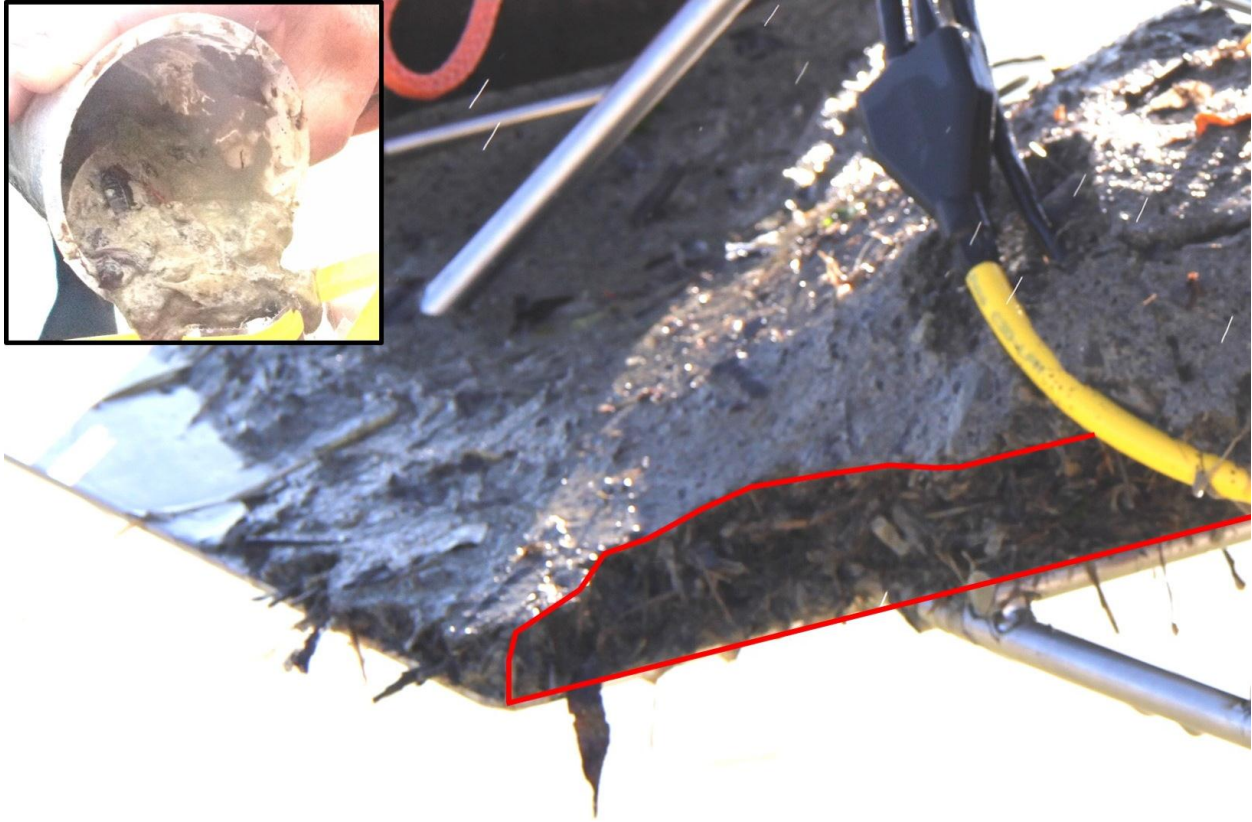


c)



d)

Figure 8. Bathymetry (a) before the summertime (September 2013) and (b) after (February 2014) the wintertime experiments. Seabed variation (c) between May and September 2013 and (d) between September 2013 and February 2014.



931

932 Figure 9. Shown is a photograph of the base of the quadpod immediately after recover from QR3. The red  
933 outline highlights a mat of fine-grained sediments and organic material that was deposited during the  
934 deployment. The inset (upper left) shows leaves mixed with fine cohesive sediments from a diver grab  
935 sample taken at QR1 prior to the storm of 24-25 January 2014.

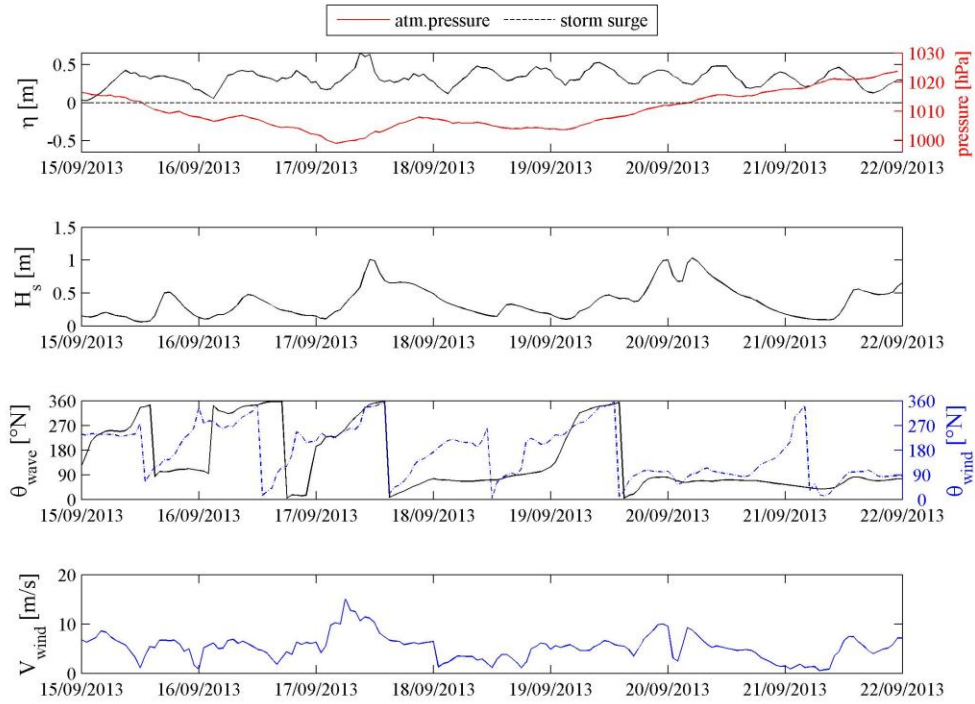
936

937 Table 4 - Median grain size  $d_{50}$  ( $\mu\text{m}$ ) of flocculated sediments at different times and locations along the  
 938 final reach of the MR. Several samples were collected at the location where the quadpod was placed and  
 939 these are denoted by QR#. The sediment samples were collected at the specified dates and then  
 940 transported to a laboratory where dynamic floc sizes were determined in a CILAS 1190 Particle Size  
 941 Analyzer at three different flow velocities.

<i>Sampling date</i>	<i>Distance from MR mouth [m]</i>	<i>Low Flow</i>	<i>Transitional Flow</i>	<i>Turbulent Flow</i>
<b>26/01</b>	525 - QR1	33.0	11.6	8.2
<b>26/01</b>	400 - QR2	31.9	13.9	10.3
<b>26/01</b>	280 - QR3	46.6	15.9	23.4
<b>26/01</b>	190	103.2	18.1	10.9
<b>27/01</b>	789	24.5	9.8	7.2
<b>27/01</b>	620	12.0	8.0	7.0
<b>27/01</b>	525 - QR1	13.3	9.0	7.3
<b>27/01</b>	525 - QR1	18.4	10.2	7.8
<b>27/01</b>	400 - QR2	9.8	7.1	6.5
<b>29/01</b>	525 - QR1	16.4	9.6	6.9
<b>29/01</b>	400 - QR2	13.2	8.8	7.1

942





943

944 Figure 10. Climate during the summertime experiment. From top to bottom: atmospheric  
 945 pressure (solid red line, from pressure gauge at the Ancona harbor) and storm surge (from the  
 946 tide gauge at the Ancona harbor); modeled significant wave height; modeled incoming direction  
 947 of waves and winds; modeled wind velocity.

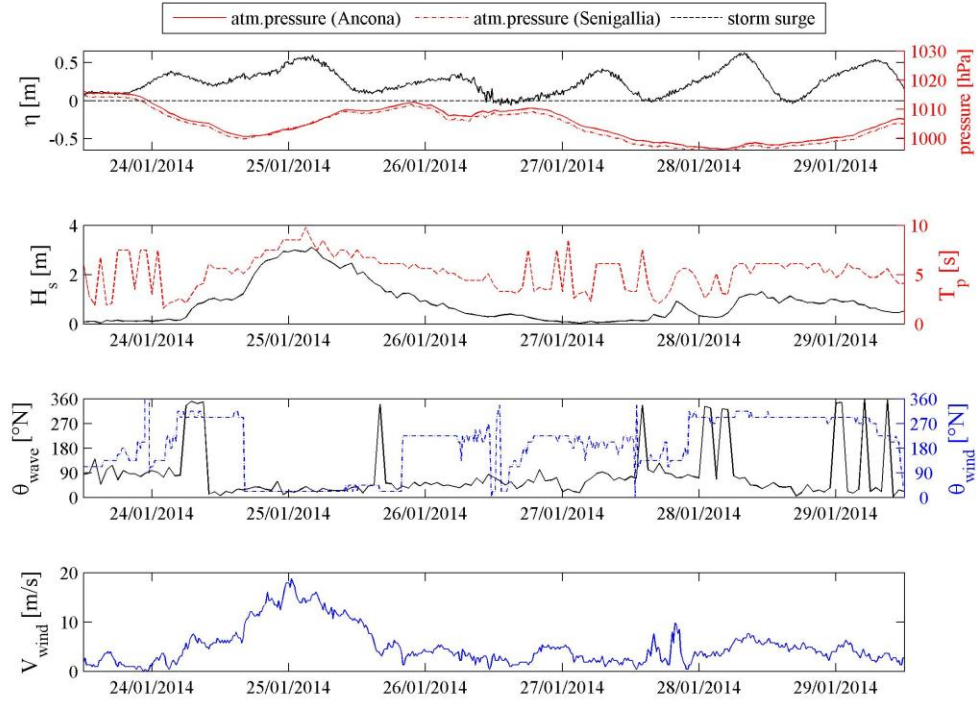


Figure 11. Climate during the wintertime experiment. From top to bottom: atmospheric pressure measured in Ancona (solid red line, from pressure gauge at the Ancona harbor) and Senigallia (dashed red line, from the local weather station) and storm surge (from the tide gauge at the Ancona harbor); measured significant wave height and peak period (from ADCP at QS3); measured incoming direction of waves (from ADCP at QS3) and winds (from weather station); measured wind velocity (from the weather station).

955

Table 5 - Surface flow features during summertime and wintertime experiments.

	stroke	Summertime (September 2013)	Wintertime (January 2014)
mean speed [m/s]	1	0.168±0.141	0.294±0.078
	2	0.111±0.072	0.377±0.115
	3	0.271±0.119	0.445±0.142
direction/course [°N]	1	79.28±99.02	14.57±32.17
	2	128.72±123.30	32.65±11.78
	3	307.20±93.24	22.55±9.66
temperature [°C]	all	21.23±1.52	8.76±1.53

956

957

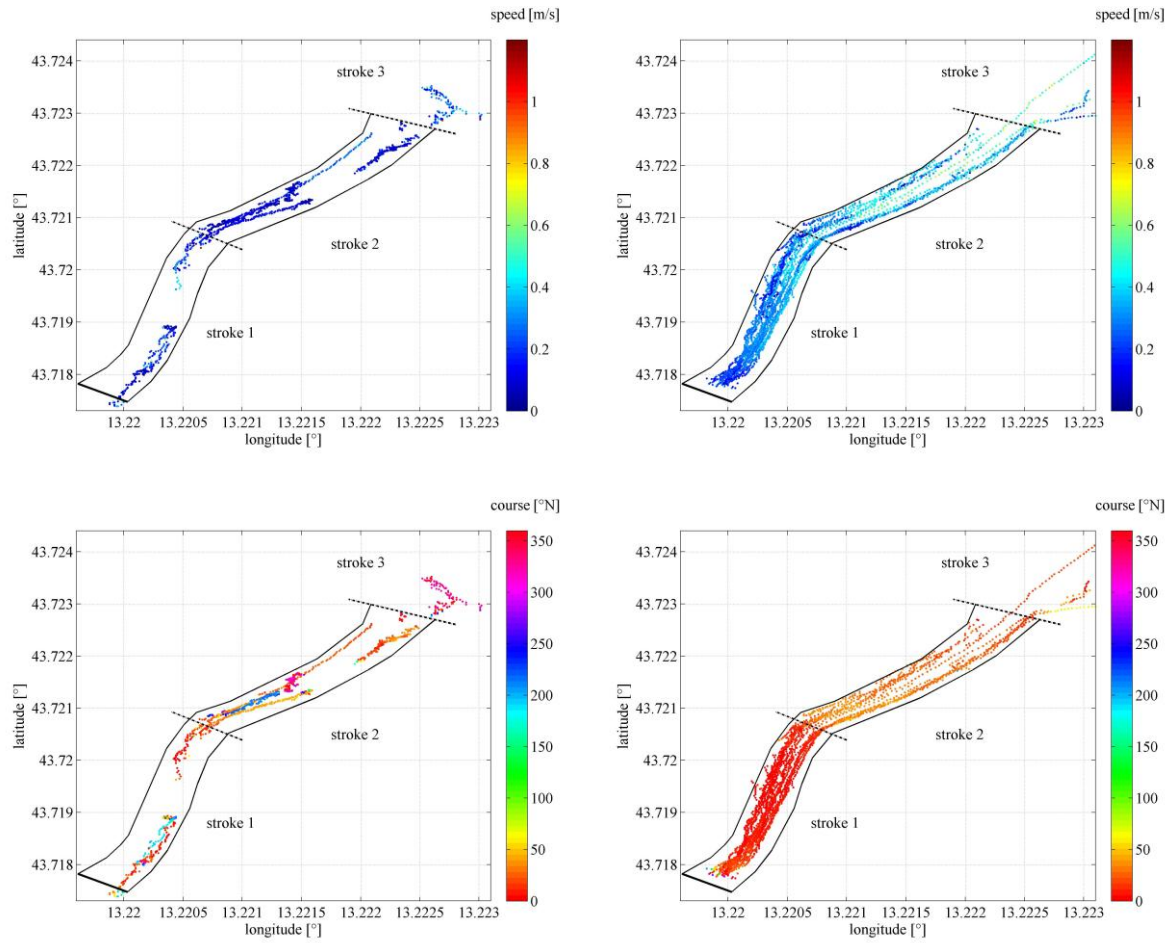


Figure 12. Shown is a compilation of drifter tracks denoting the flow speed (top) and direction (bottom) during the summertime (left panels) and wintertime (right panels) experiments. The railway bridge location is illustrated at the bottom left edge of each panel (solid thick line), while dash-dotted lines separate the three strokes.